Nonlinear self-accelerating beams induced in multilevel atomic vapors

Zhenkun Wu (wuzk1121@163.com)
Henan University
Yagang Zhang
Henan University
Kaibo Yang
Henan University
Jingmin Ru
Henan University
Feng Wen
Xi'an Jiaotong University
Yuzong Gu
Henan University

Research Article

Keywords: Nonlinear atomic vapors, Nonlinear self-accelerating beams, Under-healing effect, Over-healing effect, Self-healing effect

Posted Date: November 30th, 2020

DOI: https://doi.org/10.21203/rs.3.rs-114085/v1

Nonlinear self-accelerating beams induced in multilevel atomic vapors

ZHENKUN WU,[1,*] YAGANG ZHANG,[1] KAIBO YANG,[1] JINGMIN RU,[1] FENG WEN,[2] AND YUZONG GU[1]

[1]*Institute of nano/photon materials and application & International Joint Research Laboratory of New Energy Materials and Devices of Henan Province, School of Physics and Electronics, Henan University, Kaifeng 475004, PR China;*

[2]*Key Laboratory for Physical Electronics and Devices of the Ministry of Education & School of Science & Shaanxi Key Lab of Information Photonic Technique & Institute of Wide Bandgap Semiconductors, Xi'an Jiaotong University, Xi'an 710049, PR China;*

**Corresponding author: wuzk1121@163.com;*

Abstract: We demonstrate the existence and curious propagation dynamics of self-accelerating beams in Λ-type three-level nonlinear atomic vapors with Kerr and cubic-quintic nonlinearities through numerical investigation and mathematical modelling. Upon adjusting the generation and propagation conditions, these nonlinear accelerating beams exhibit different evolution properties. We demonstrate that the input beams can propagate robustly in the medium regardless of its absorption properties. The shape and peak intensity of the main lobes of these input beams, which are the eigenmodes of the nonlinear Schrödinger equation (NLSE) in atomic media, are preserved for a significantly long propagation distance. If such beams are not the modes of the system, they are subjected to the under-healing or over-healing effect, which damages the shape of the self-accelerating beams. We also discuss the interactions between truncated accelerating beams, which readily generate non-accelerating solitons and soliton pairs. The results indicate that the atomic vapor can serve as a promising medium for the generation of nonlinear self-accelerating beams.

Extensive research on special non-solid materials, such as atomic vapor-cell systems, has led to rapid developments in areas such as quantum optics and metrology over the past few decades [1–9]. Atomic vapors have attracted enormous attention and been intensely investigated owing to their multi-parameter tunable properties. To obtain a significant suppression of optical absorption and a large reduction of group velocity in these platforms [6], electromagnetically induced transparency (EIT) window was developed. In recent years, several noteworthy phenomena have been observed in periodically dressed atomic systems. These include enhanced multi-wave mixing signals caused by Bragg reflection from

photonic bandgap structures [10], photonic topological insulators [11], cubic-quintic (CQ) condensate solitons [12], (anti-) parity-time symmetric systems [13–15], optical Bloch oscillations and Zener tunneling [16], and edge solitons in photonic graphene [17]. The dressed atomic system is a good platform for studying various self-accelerating beams because its optical properties are well-known.

Airy beams belong to the family of paraxial self-accelerating beams. They exhibit accelerating, nondiffracting, and self-healing properties and have become a subject of significant interest in the last decade [18–25]. As reported in [26], Airy beams attenuate quickly when propagating in an atomic vapors, even when the absorption by the media is small. Hence, they are not a loss-proof beams [27]. In stark contrast to the paraxial Airy beam, there exists a different type of loss-proof self-accelerating beam that can propagate robustly in atomic vapors. Loss-proof beams, such as Bessel, Weber, and Mathieu beams, belong to the family of nonparaxial accelerating beams [26–29]. The dynamics and properties of paraxial and nonparaxial accelerating beams in atomic systems have been thoroughly investigated. However, most of the research has been restricted to linear accelerating beams. In this paper, we investigate the properties of nonlinear accelerating beams.

Herein, we numerically investigate the existence and evolution of accelerating beams in a three-level nonlinear atomic configuration with Kerr as well as CQ non linearities. Our approach is novel. We found that truncated nonlinear accelerating beams can propagate in an absorbing atomic media, while preserving their peak intensity and the shape of their main lobe region over a large distance due to the intensified self-healing effect. This is in contrast to the usual scenario, where the under-healing and over-healing effects gradually attenuates and raises, respectively, the intensity of the main lobe of the truncated accelerating beams during propagation. Additionally, we also extend our investigation to the interactions between truncated accelerating beams that readily generate non-accelerating solitons and soliton pairs. Numerical investigation and mathematical modelling have been adopted in this study.

Results and discussion

Mathematical modeling and propagation equation. We begin by examining

Maxwell's equations in a three-level atomic configuration of rubidium, formed with an excited state, $|2\rangle\,(4D_{3/2})$, and two lower-level states, $|1\rangle\,(3P_{1/2})$ and $|0\rangle\,(3S_{1/2})$, as demonstrated in Fig. 1(a).

$$\vec{\nabla}\cdot\vec{E}=0,\ \vec{\nabla}\cdot\vec{B}=0,\ \vec{\nabla}\times\vec{E}=-\frac{\partial\vec{B}}{\partial t},\ \vec{\nabla}\times\vec{B}=-\varepsilon_0\mu_0(1+\chi)\frac{\partial\vec{E}}{\partial t}\ , \tag{1}$$

where $\chi=\sum_{j=0}^{2}\chi^{(2j+1)}|E|^{2j}$, μ_0 is the permeability in vacuum, and ε_0 is the permittivity. $\chi^{(1)}$, $\chi^{(3)}$, and $\chi^{(5)}$ represent the linear, the third-order, and the fifth-order susceptibility indices, respectively. From Eq. (1) we derive the wave equation in multilevel atomic vapors with linear and nonlinear gain or loss.

$$\nabla^2\vec{E}=\varepsilon_0\mu_0\frac{\partial^2\vec{E}}{\partial t^2}+\varepsilon_0\mu_0(\chi^{(1)}+\chi^{(3)}|E|^2+\chi^{(5)}|E|^4)\frac{\partial^2\vec{E}}{\partial t^2} \tag{2}$$

Herein, the two-dimensional case is considered. Thus, the TE-polarized solution of Eq. (2) is written as $\vec{E}(x,y,z)=E_y(x,z)\hat{y}$. We seek solutions in the harmonic form $\vec{E}=\psi(x,\,z)\exp(ikz-i\omega t)\hat{y}$, where $k=\omega/c$ is the wave number, and ω is the wave frequency. Under the paraxial approximation $|\partial_z^2\psi|\ll|2k\partial_z\psi|$, the paraxial wave equation is obtained as

$$i\frac{\partial}{\partial z}\psi+\frac{1}{2k}\frac{\partial^2}{\partial x^2}\psi+\frac{k}{2}\chi\psi=0 \tag{3}$$

The linear and nonlinear susceptibility indices can be obtained through the Liouville pathways using perturbation theory [30]:

$$\chi^{(1)}=\frac{iN\mu_{10}^2}{\hbar\varepsilon_0}\frac{1}{K},\qquad \chi^{(3)}=\frac{-iN\mu_{10}^4}{\hbar^3\varepsilon_0}\frac{1}{K^2d},\qquad \chi^{(5)}=\frac{iN\mu_{10}^6}{\hbar^5\varepsilon_0}\frac{1}{K^3d^2}, \tag{4}$$

where $K=\Gamma_{10}+i\Delta_1+|G_2|^2/d$ and $d=\Gamma_{20}+i(\Delta_1-\Delta_2)$. $G_2=\mu_{12}E_2/\hbar$ is the Rabi frequency of the control field, μ_{ij} is the transition electric dipole moment between levels $|i\rangle$ and $|j\rangle$, N is the atomic density, and Γ_{ij} denotes the rate at which the population decays from state $|i\rangle$ to state $|j\rangle$. $\Delta_1=\omega_1-\omega_{10}$ and $\Delta_2=\omega_2-\omega_{21}$ are the probe and control field detuning, respectively, where the atomic resonant frequency and the laser frequency are represented by $\omega_i(i=1,2)$ and $\omega_{ij}(j=0,1)$, respectively. Fig. 1(b) shows the real and imaginary parts of linear $\chi^{(1)}$—$\mathrm{Re}\chi^{(1)}$ and $\mathrm{Im}\chi^{(1)}$, respectively—as functions of Δ_1. Clearly, an EIT window

is opened in the probe-field absorption spectrum $\mathrm{Im}\chi^{(1)}$ near $\Delta_1 = 0$. Hence, the probe field can propagate in the system with nearly vanishing absorption. In addition, the slope of $\mathrm{Re}\chi^{(1)}$ is drastically steepened, resulting in a significantly slow propagation of the probe field.

For technical convenience, we introduce the transformation of coordinates $\xi = \sqrt{k}\,x$ in Eq. (3) to obtain Eq. (5).

$$i\frac{\partial\psi(\xi,z)}{\partial z} + \frac{1}{2}\frac{\partial^2\psi(\xi,z)}{\partial\xi^2} + \frac{k}{2}\chi\psi(\xi,z) = 0 \tag{5}$$

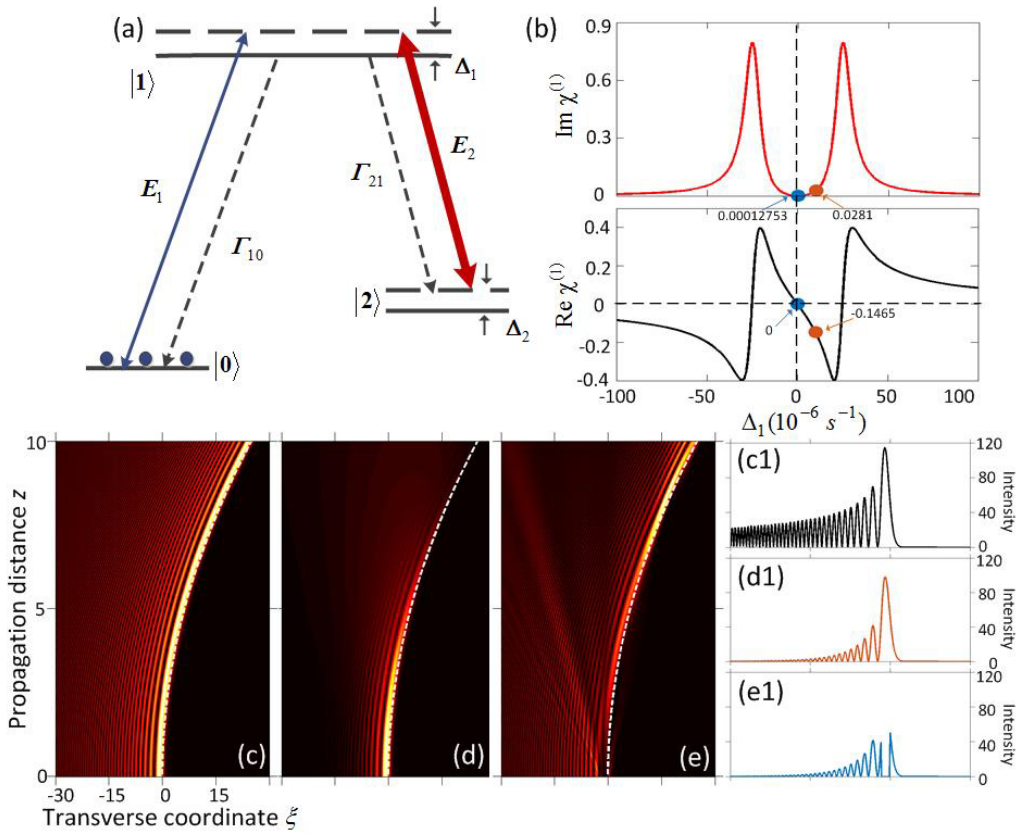

Fig. 1. (Color online) (a) Energy-level diagram and excitation scheme of Λ-type three-level atoms interacting with a weak pulsed probe field E_1 and a strong continuous-wave control field E_2. (b) $\mathrm{Im}\chi^{(1)}$ (upper graph) and $\mathrm{Re}\chi^{(1)}$ (lower graph) as functions of Δ_1 for $G_2 = 25\times10^6\ s^{-1}$ and $\Delta_2 = 0$. The conditions $\Delta_1 = 0$ and $\Delta_1 = 10\times10^6\ s^{-1}$ are indicated by the blue and orange dots, respectively. The parameters are set as follows: $\lambda = 532\ nm$, $N = 5\times10^{13}\ cm^{-3}$, $\mu_{10} = 1.22\times10^{-29}\ C\cdot m$, and $\Gamma_{10} = 10\times10^6\ s^{-1}$. Propagation of (c) the ideal Airy beam and (d) truncated Airy beam with $a = 0.08$ according to the LSE. (e) Self-healing process of the truncated Airy beam. The white dashed line is the theoretical trajectory. (c1)-(e1) Cross-sections of the beam intensity at $z = 0$ corresponding to (c)-(e),

respectively.

Case A: Ordinary Airy beam in the linear schrödinger equation. Neglecting the term $k\chi/2$, Eq. (5) is the linear Schrödinger equation (LSE). By applying the Fourier transform (FT) to the LSE, the following equation is obtained:

$$i\frac{\partial}{\partial z}\hat{\psi}(\omega,z)=\frac{1}{2}\omega^2\hat{\psi}(\omega,z), \tag{6}$$

where ω is the spatial frequency. The FT used here is defined in Eq. (7).

$$\hat{\psi}=\int_{-\infty}^{+\infty}\psi\times e^{-i\omega\xi}d\xi, \qquad \psi=\frac{1}{2\pi}\int_{-\infty}^{+\infty}\hat{\psi}\times e^{i\omega\xi}d\omega. \tag{7}$$

The solution to Eq. (6) is of the general form $\hat{\psi}(\omega,z)=\hat{\psi}(\omega,0)\exp(-1/2i\omega^2 z)$ [30–34]. To obtain the corresponding solution in the real space, it is necessary to perform an inverse FT on the solution of Eq. (6), as follows:

$$\psi(\xi,z)=\frac{1}{2\pi}\int_{-\infty}^{+\infty}\hat{\psi}(\omega,0)\times e^{-\frac{i\omega^2 z}{2}}\times e^{i\omega z}d\omega, \tag{8}$$

where $\hat{\psi}(\omega,0)$ is the FT of the input beam. Clearly, the structure of a given beam at any propagation distance z can be solved numerically. Here, the ideal Airy beam is considered as the input.

$$\psi(\xi,0)=Ai(\xi) \tag{9}$$

The propagation of the ideal Airy beam is shown in Fig. 1(c). The beam accelerates along a parabolic trajectory (the white dashed line) with the characteristic infinite oscillatory tail owing to its infinite energy. To make the energy of the Airy wave finite, we truncate the ideal Airy beam as $\psi(\xi,\ 0)=Ai(\xi)\exp(a\xi)$, with an arbitrary real decay constant $a\geqslant 0$. The corresponding propagation is shown in Fig. 1(d). Clearly, the tail of the truncated beam quickly decays during propagation, preserving the nondiffracting and self-accelerating properties only over a finite distance. Fig. 1(e) shows the evolution of the beam and reveals the self-healing property. The main lobe of the beam is screened out initially, but it recovers quickly with increase in the propagation distance because of the energy transfer from the tail to the head of the beam. The input intensity profiles corresponding to Figs. 1(c)–1(e) are represented in Figs. 1(c1)–1(e1), respectively.

Case B: Accelerating beam in atomic vapor with Kerr nonlinearity. By introducing

the Kerr-type focusing nonlinearity $\chi \propto \chi^{(3)}|\psi|^2$ in Eq. (5), we address the nonlinear accelerating solutions of Kerr NLSE. ξ in Eq. (5) is substituted by a traveling variable $\xi - z^2/4$ [20, 35] to obtain Eq. (10).

$$i\frac{\partial \psi}{\partial z} - i\frac{z}{2}\frac{\partial \psi}{\partial \xi} + \frac{1}{2}\frac{\partial^2 \psi}{\partial \xi^2} + \frac{k}{2}\chi^{(3)}|\psi|^2\psi = 0 \tag{10}$$

We are interested in nonlinear self-trapped solutions of Eq. (10) of the form $\psi(\xi, z) = u(\xi)\exp[i(\xi z/2 + z^3/24)]$, accelerating along a parabolic trajectory. After some algebra, we obtain

$$\frac{\partial^2 u}{\partial \xi^2} + k\chi^{(3)}|u|^2 u - \xi u = 0 \tag{11}$$

We use the analytical Airy solution of the linear equation to set the boundary conditions [20, 28]: $u(\xi) = \alpha Ai(\xi)$ and $u'(\xi) = \alpha Ai'(\xi)$. Here, α indicates the strength of the nonlinearity induced by the potential solution, and $Ai'(\xi) = -\xi K_{2/3}\left(\frac{2}{3}\xi^{3/2}\right)/\left(\sqrt{3}\pi\right)$, where $K_\nu(\xi)$ is the νth-order modified Bessel function [36]. With the boundary conditions, the eigenfunction Eq. (11) can be solved numerically. We first consider the Kerr accelerating solution at the EIT condition [7–9] (indicated by the blue dot), i.e., $\Delta_1 = \Delta_2 = 0$. As shown in Fig. 2(a), the Kerr nonlinearity index is calculated to be $\chi^{(3)} \approx -i2.7293 \times 10^{-9}\ m^2 \cdot W^{-1}$. This value is indeed small and leads to losses in the beam propagation. In Fig. 2(b), we compare the intensities of the linear Airy mode $3.5Ai(\xi)$ and the nonlinear Kerr accelerating mode with $\alpha = 1000$ at $z = 0$. The Kerr accelerating mode (the blue curve) exhibits long tails and possesses infinite energy. It is similar in shape to the Airy mode (the orange curve), but has lobes with different intensities.

When using it as the input beam, we truncate the Kerr nonlinear accelerating solution directly after 25 lobes. With the split-step Fourier propagation method, the propagation properties of the truncated beam can be numerically derived by solving Eq. (5) directly under the propagation condition $\Delta_1 = \Delta_2 = 0$, as shown in Fig. 2(c). It is clear that the beam evolution exhibits self-accelerating and nondiffracting properties, following a parabolic trajectory (the white dashed curve), and that the beam shape is preserved. Even though there is absorption, as an eigenmode of the

system, the energy from the beam's tail transfers to the main lobe, which then preserves the beam shape. In Fig. 2(d), we show the propagation of the same input beam used in Fig. 2(c) but with evolution under the condition $\Delta_1 = 10$ MHz and $\Delta_2 = 0$ (indicated by the orange dot in Fig. 2 (a)). This condition corresponds to the nonlinearity index $\chi^{(3)} \approx -i1.3765 \times 10^{-6} + 3.4691 \times 10^{-6}\ m^2 \cdot W^{-1}$, which leads to a significantly larger absorption than that under the $\Delta_1 = \Delta_2 = 0$ condition. The corresponding beam propagation is shown in Fig. 2(d), in which the beam attenuates gradually, and its shape is modified. This happens because such a beam is not an eigenmode of the propagation described in Eq. (5) any longer. During propagation, the tail eventually becomes too high to maintain the main lobe and compensate for the large absorption. The beam evolution shown in Fig. 2(d) indicates the under-healing effect [26, 27]. The truncated Kerr accelerating beam is then set with an initial velocity $v_{in} = v_0 \xi$. Similar to Figs. 2(c) and 2(d), the propagation dynamics of the tilted beam are shown in Figs. 2(e) and 2(f) with $v_0 = 3$. Clearly, the oblique Kerr nonlinear accelerating beam still accelerates along a parabolic curve upon propagation, but the trajectory of this truncated beam is determined by $\xi = 3z + z^2/4$ (the white dashed curve).

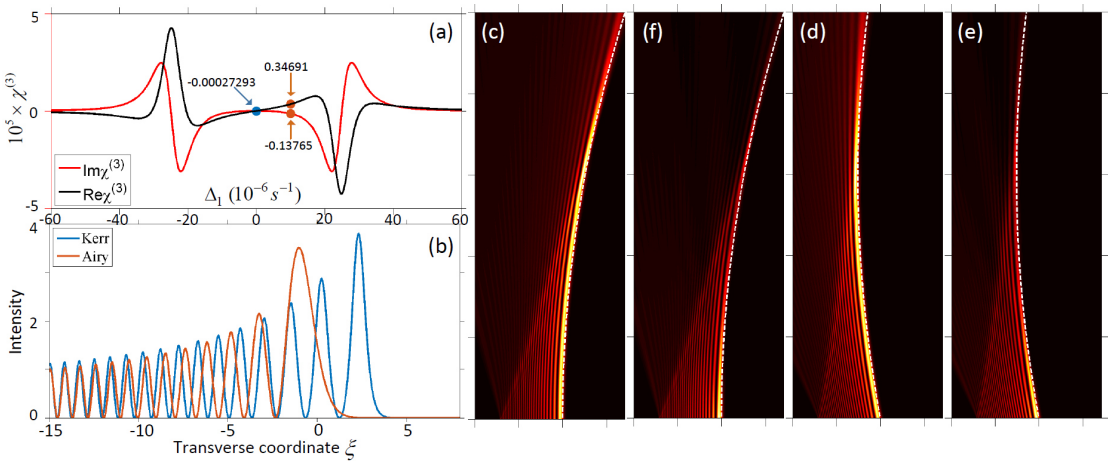

Fig. 2. (Color online) (a) $\mathrm{Im}\chi^{(3)}$ (red curve) and $\mathrm{Re}\chi^{(3)}$ (black curve) as functions of Δ_1 at $G_2 = 25 \times 10^6\ s^{-1}$ and $\Delta_2 = 0$. (b) Intensities of the Airy beam and the nonlinear Kerr accelerating solution at $z = 0$. (c) Propagation of the truncated Kerr accelerating eigenmode in the nonlinear medium with $\Delta_1 = \Delta_2 = 0$. (d) Propagation of the same beam, but in the nonlinear medium with $\Delta_1 = 10$ MHz and $\Delta_2 = 0$. The white dashed curves show the analytical trajectory. (f) and (e) Accelerations of the truncated Kerr beam with an initial velocity

$v_0 = 3$, with (f) $\Delta_1 = \Delta_2 = 0$ and (e) $\Delta_1 = 10$ MHz and $\Delta_2 = 0$.

In Fig. 3(a), the peak intensities of the truncated beam in both cases are recorded during propagation. It can be seen from Fig. 3(a) that the beam in Fig. 2(e) maintains its peak intensity well, while that in Fig. 2(f) decays appreciably owing to the large absorption. In addition, as presented in Fig. 3(b), the evolution of the truncated Kerr accelerating beam also displays the unique self-healing property in the absorbing atomic system. Fig. 3(c) shows the truncated eigensolution and its propagation under the condition $\Delta_1 = 10$ MHz and $\Delta_2 = 0$, while Fig. 3(d) presents the evolution of the same beam under the condition $\Delta_1 = \Delta_2 = 0$. As expected, in Fig. 3(c), the eigenmode propagates robustly in the medium, maintaining its intensity and accelerating along a parabolic trajectory, which is quite similar to the beam propagation shown in Fig. 2(e). More interesting propagation properties are exhibited in Fig. 3(d). Clearly, although the parabolic trajectory of acceleration is still presented during the propagation, the intensity of the main lobe continued to grow significantly until the beam's tail is completely used up. This happens due to the over-healing effect [26, 27]. The absorption of the system is smaller than that in the case shown in Fig. 3(c), and the energy transferred from the tail to the main lobe over-compensates the absorption. The peak intensities recorded during the beam evolution also demonstrate the above analysis, as shown in Fig. 3(f).

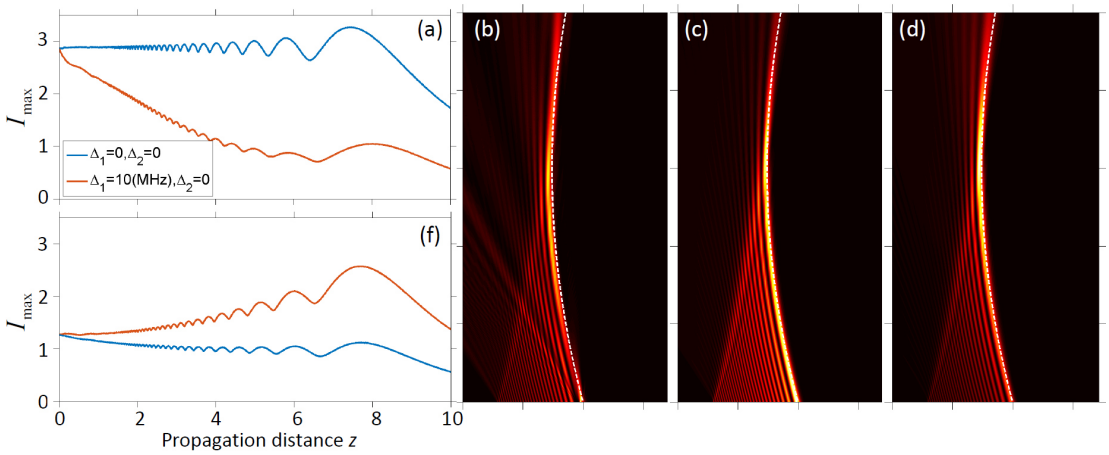

Fig. 3. (Color online) (a) Peak intensities of the truncated Kerr accelerating beam during propagation. The blue curve and the orange curve correspond to Figs. 2 (c) and 2(d), respectively. (b) Self-healing process of the truncated beam. (c) Propagation of the truncated Kerr accelerating eigenmode in the nonlinear medium with $\Delta_1 = 10$ MHz and $\Delta_2 = 0$. (d) Propagation of the same beam in the nonlinear medium with $\Delta_1 = \Delta_2 = 0$. (f) Peak intensities of beams shown in

Figs. 3(c) and 3(d) during propagation.

Case C: Accelerating beam in atomic vapor with cubic-quintic nonlinearity. In this subsection, we consider the nonlinearity of the atomic medium to be of the competing CQ type, in which the cubic and quintic susceptibilities are presented simultaneously. So that the nonlinearity is $\chi \propto \chi^{(3)}|\psi|^2 + \chi^{(5)}|\psi|^4$. Eigenfunction Eq. (11) is rewritten as

$$\frac{\partial^2 u}{\partial \xi^2} + k(\chi^{(3)}|u|^2 + \chi^{(5)}|u|^4)u - \xi u = 0 \tag{12}$$

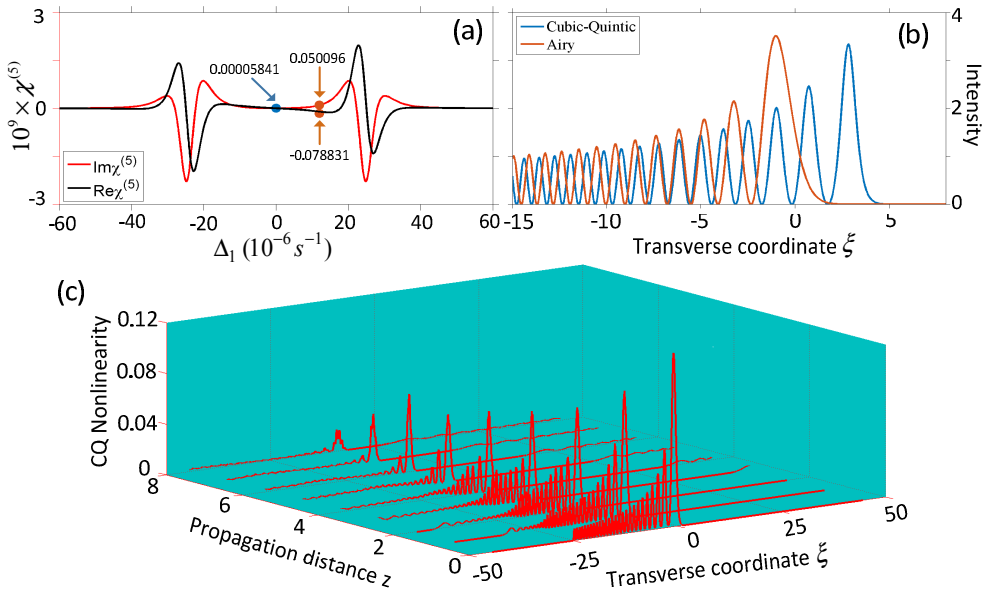

Fig. 4. (Color online) (a) Plot of $\chi^{(5)}$ as functions of Δ_1 at $G_2 = 25 \times 10^6\ s^{-1}$ and $\Delta_2 = 0$. (b) Intensities of the Airy beam and the CQ nonlinear accelerating solution at $z = 0$. (c) Plot of the nonlinearitiy in the CQ medium with propagation distance.

Similar to the case of the Kerr nonlinearity, the CQ nonlinearity also yields a nonlinear accelerating solution. Fig. 4(a) shows the dependencies of the real and imaginary parts of the CQ nonlinearity index $\chi^{(5)}$ on Δ_1. The blue and orange dots characterizing the index $\chi^{(5)}$ are calculated as $\chi^{(5)} \approx i5.8410 \times 10^{-14}\ m^4 \cdot W^{-2}$ and $\chi^{(5)} \approx i5.0096 \times 10^{-11} - 7.8831 \times 10^{-11}\ m^4 \cdot W^{-2}$, respectively. For $\Delta_1 = \Delta_2 = 0$, Fig. 4(b) compares the nonlinear CQ accelerating eigensolution and linear Airy mode, from which the similarity in shape between the two beams is visible. We emphasize that the differences are naturally defined by the nonlinear gain or loss. For further clarification, in Fig. 4(c), we illustrate the imaginary parts of $k\chi/2$ in the CQ medium upon propagation, which affect the evolution of the truncated accelerating

beam. As displayed in Fig. 4(c), with increasing propagation distance, the CQ nonlinearity gets attenuated gradually, preserving the beam shape.

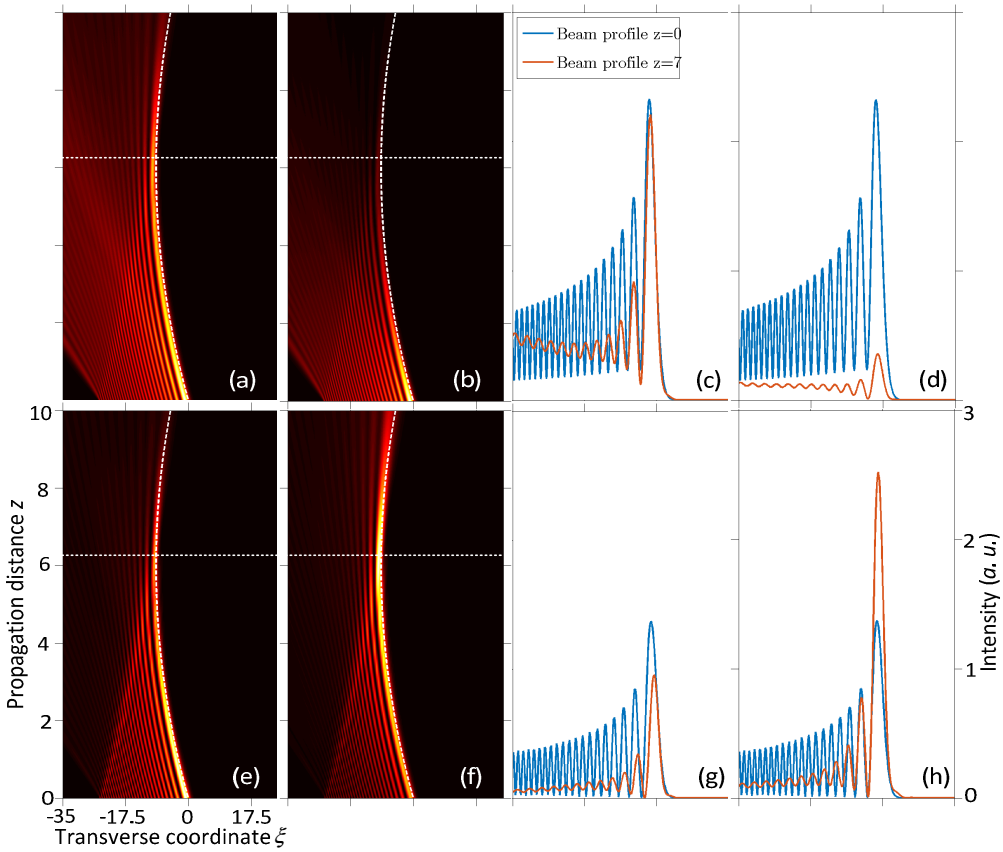

Fig. 5. (a) Propagation of the truncated CQ accelerating eigenmode in the nonlinear medium with $\Delta_1 = \Delta_2 = 0$. (b) Propagation of the same beam, but in the nonlinear medium with $\Delta_1 = 10\ \mathrm{MHz}$ and $\Delta_2 = 0$. (c) and (d) Beam profiles of (a) and (b) at propagation distance $z = 0$ and $z = 7$. The propagation of the truncated eigenmode with $\Delta_1 = 10\ \mathrm{MHz}$ and $\Delta_2 = 0$, and then (f) $\Delta_1 = \Delta_2 = 0$. (g) and (h) Beam profiles of (e) and (f) at propagation distance $z = 0$ and $z = 7$.

In Fig. 5, the propagation properties of truncated CQ nonlinear accelerating beams are summarized. Specifically, Fig. 5(a) shows the truncated eigenmode of Eq. (12) and its propagation under the condition $\Delta_1 = \Delta_2 = 0$. Fig. 5(c) shows the profile of the propagating beam at $z = 0$ and at $z = 7$. As expected, the peak intensity and the structure of this beam's main lobe are maintained over large distances. It is evident that the main lobe of the beam is robust during propagation. In contrast, in the truncated mode propagation of the same beam under the condition $\Delta_1 = 10\ \mathrm{MHz}$ and $\Delta_2 = 0$, the beam attenuates gradually owing to the under-healing effect, as depicted in Fig. 5(b). Fig. 5(d) presents the profile of this

beam at $z=0$ and at $z=7$. Similar to Figs. 3(c) and 3(d) in Kerr-type nonlinearity case, in Figs. 5(e)–5(h), the truncated accelerating beam for different CQ type nonlinearities that travel along parabolic trajectories are shown. The shape preservation of the beam and the over-healing effects are also confirmed by these results.

Interactions of nonlinear accelerating beams. Similar to the interactions of Airy beams [20, 22, 37], we address the interactions of nonlinear accelerating beams induced in a coherent atomic system. Since the nonlinear accelerating beams possess infinite oscillating tails, we discuss interactions between truncated beams with finite energies. The incident beams are written as [20, 37]

$$\psi(\xi)=\psi_1[(\xi-\xi_0)]+\mathrm{e}^{il\pi}\psi_2[-(\xi+\xi_0)], \tag{13}$$

where ψ_1 and ψ_2 are the two truncated nonlinear solutions. ξ_0 is the transverse position shift and l is the parameter controlling the phase shift. If $l=0$, the two components are in-phase. If $l=1$, the two components are out-of-phase.

Case A: Kerr Medium. The interactions of two truncated nonlinear beams in Kerr medium are studied. Fig. 6 shows the interactions of two in-phase (top row) and out-of-phase (bottom row) truncated Kerr beams obtained with $\alpha=1000$. Clearly, solitons and solitons pairs can be produced from the interactions. The reason is clear: the two components coincide with each other and the amplitude of the superposed beam is doubled, so that the main lobes as well as the shedding radiation can form solitons. It should be noted in Figure 6(d1), with $\xi_0=1$ the energy is highly concentrated in the middle, and a soliton chain is formed, and the Kerr nonlinearity has played a major role. It is worth noting that the solitons and soliton pairs exhibit particle properties and do not accelerate. Figs. 6(a1), 6(g1), 6(a2), and 6(g2) indicate that with the increasing interval between the two components, the interaction becomes weak gradually.

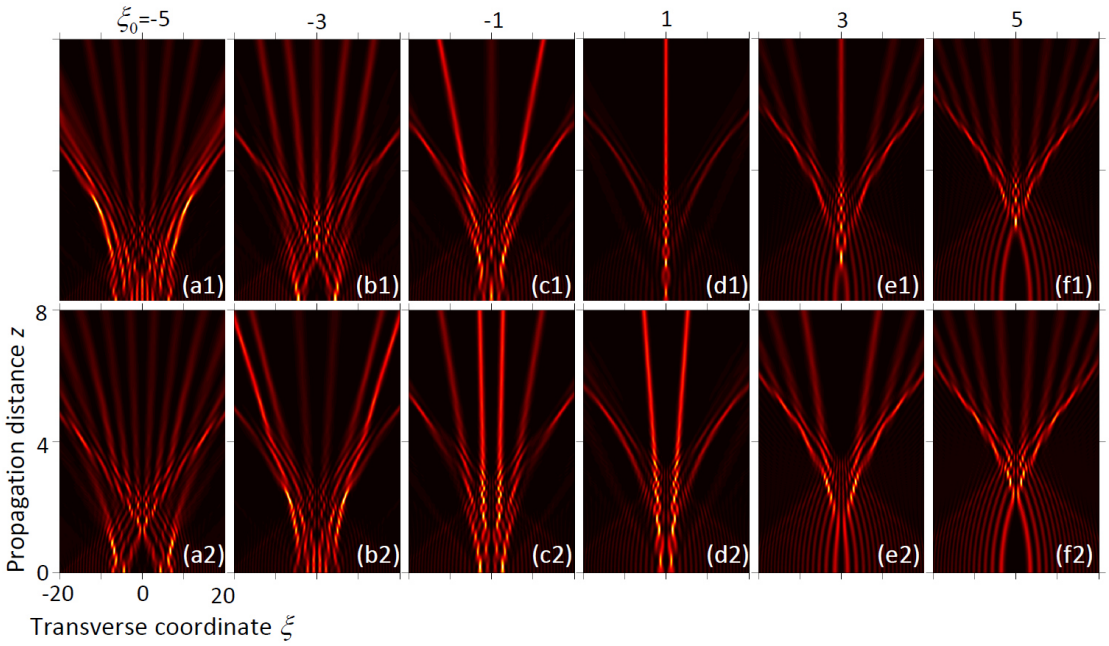

Fig. 6. (Color online) Interaction of two in-phase (top row) and out-of-phase (bottom row) truncated Kerr accelerating beams and their propagation under the condition $\Delta_1 = \Delta_2 = 0$.

Case B: Cubic-Quintic Medium. Figs. 7(a1)–7(f1) and 7(a2)–7(f2) depict the in-phase (top row) and out-of-phase (bottom row) interactions of the two truncated CQ nonlinear solutions, respectively. It can be seen that it is difficult for the accelerating beams to generate non-accelerating single solitons and soliton pairs. Less soliton pairs are induced from the CQ solutions when compared to the truncated Kerr solutions. As mentioned above, the interactions are relatively weak if the two components are far away, as shown in Figs. 7(a1) and 7(a2).

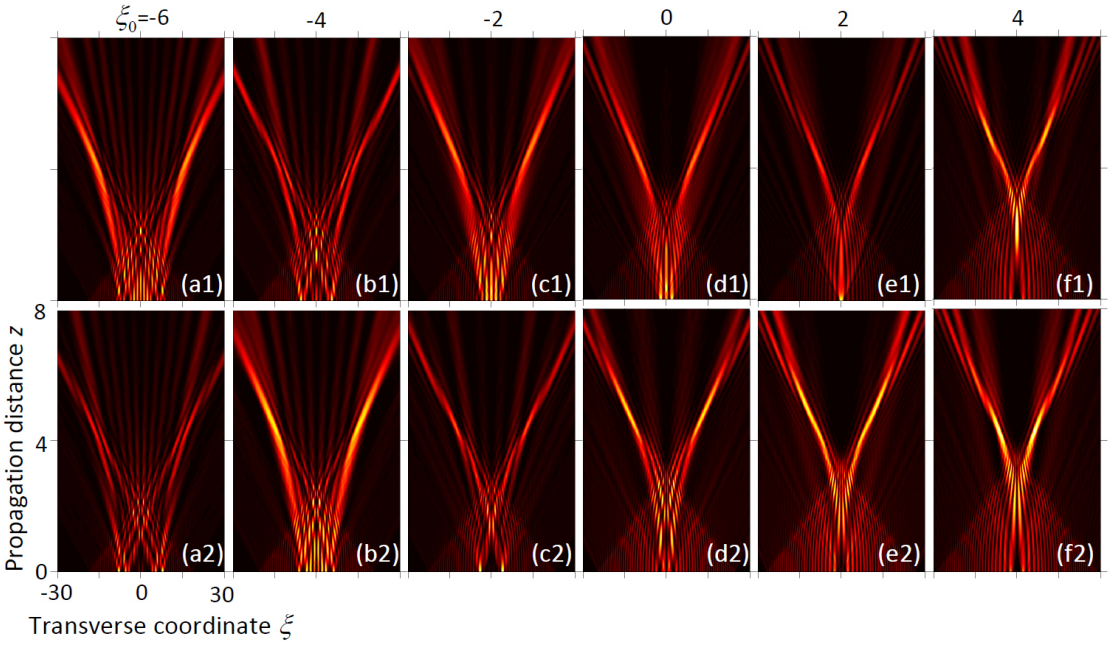

Fig. 7. (Color online) Interaction of two in-phase (top row) and out-of-phase (bottom row) truncated CQ accelerating beams and their propagation under the condition $\Delta_1 = \Delta_2 = 0$.

Conclusion

In summary, we reported on the existence and evolution of self-accelerating beams in a three-level atomic configuration with Kerr and CQ nonlinearities. These truncated accelerating eigenmodes propagate in absorbing atomic media, with both their shape and the peak intensity of their main lobe preserved for a considerably long propagation distance. This behavior originates from the intensified self-healing effect. Otherwise, the under-healing or over-healing effect will gradually attenuate or raise the intensity of the main lobe of the beams during the propagation. In addition, we studied the interactions of truncated Kerr beams and truncated CQ nonlinear accelerating beams. During the beam interactions, non-accelerating solitons and soliton pairs, that exhibit particle properties, could be readily generated. These results of this study indicate that the atomic vapor can serve as a promising medium for the generation of nonlinear self-accelerating beams. Conversely, nonlinear self-accelerating beams may lead to new ideas in the study of atomic media and atomic ensembles. Our research may broaden the field of potential applications of self-accelerating beams and can be applied for particle acceleration and ignition of intensity-driven nonlinear processes.

Methods

Split-step fast Fourier transform method. To study the formation and dynamics of vortices we solve propagation Eq. (5) numerically by the fourth-order split-step fast Fourier transform (FFT) method in double precision, which is used to integrate the nonlinear Schrödinger equation. This method relies on computing the solution in small steps, and treating the linear and the nonlinear steps separately. Firstly, we rewrite Eq. (5) as:

$$\frac{\partial \psi}{\partial z} = \left(\hat{D} + \hat{N}\right)\psi, \tag{14}$$

with $\hat{D}$ and $\hat{N}$ are the linear and nonlinear operator,

$$\hat{D} = i\frac{1}{2}\frac{\partial^2}{\partial \xi^2} \tag{15a}$$

$$\hat{N} = i\frac{k}{2}\chi \tag{15b}$$

respectively. For an optical beam $\psi(\xi,z)$ at propagation distance z, in the next step dz, the optical field distribution $\psi(\xi,z+dz)$ can be obtained with the Split-step method. In the first half of the step $dz/2$, we only consider the effect of the linear operator

$$\psi_D(\xi,z+dz/2) = \exp\left(\hat{D}dz/2\right)\psi(\xi,z) \tag{16}$$

and then we consider the nonlinear operator in the whole step dz

$$\psi_N(\xi,z+dz/2) = \exp\left(\hat{N}dz\right)\psi_D(\xi,z+dz/2) \tag{17}$$

finally, in the second half of the step $dz/2$, the linear operator is considered again and the optical field distribution $\psi(\xi,z+dz)$ can be obtained as

$$\psi(\xi,z+dz) = \exp\left(\hat{D}dz/2\right)\exp\left(\hat{N}dz\right)\exp\left(\hat{D}dz/2\right)\psi(\xi,z) \tag{18}$$

Data avaliability

The data that supports the results of this work are available from the corresponding author upon reasonable request.

REFERENCES

[1] Hemmer, P. et al. Efficient low-intensity optical phase conjugation based on coherent population trapping in sodium, *Opt. Lett.* **20**, 982 (1995).

[2] Jain, M. et al. Efficient nonlinear frequency conversion with maximal atomic coherence, *Phys. Rev. Lett.* **77**, 4326 (1996).

[3] Harris, S. Electromagnetically induced transparency, *Phys. Today.* **50**, 36 (1997).

[4] Lukin, M. et al. Quantum Noise and Correlations in Resonantly Enhanced Wave Mixing Based on Atomic Coherence, *Phys. Rev. Lett.* **82**, 1847 (1999).

[5] Kang, H. et al. Resonant four-wave mixing with slow light, *Phys. Rev. A.* **70**, 061804 (2004).

[6] Fleischhauer, M. et al. Electromagnetically induced transparency: Optics in coherent media, *Rev. Mod. Phys.* **77**, 633 (2005).

[7] Zhang, Y. et al. Opening four-wave mixing and six-wave mixing channels via dual electromagnetically induced transparency windows, *Phys. Rev. Lett.* **99**, 123603

(2007).

[8] Zhang, Y. et al. Four-wave mixing dipole soliton in laser-induced atomic gratings, *Phys. Rev. Lett.* **106**, 093904 (2011).

[9] Zhang, Y. et al. Modulated vortex solitons of four-wave mixing, *Opt. Express.* **18**, 10963 (2010).

[10] Zhang, Y. et al. Controlling multi-wave mixing signals via photonic band gap of electromagnetically induced absorption grating in atomic media, *Opt. Express.* **21**, 29338 (2013).

[11] Zhang, Y. et al. Photonic Floquet topological insulators in atomic ensembles, *Laser Photon. Rev.* **9**, 331 (2015).

[12] Wu, Z. et al. Cubic-quintic condensate solitons in four-wave mixing, *Phys. Rev. A.* **88**, 063828 (2013).

[13] Hang, C. et al. *PT* symmetry with a system of three-level atoms, *Phys. Rev. Lett.* **110**, 083604 (2013).

[14] Peng, P. et al. Anti-parity–time symmetry with flying atoms, *Nat. Phys.* **12**, 1139 (2016).

[15] Zhang, Z. et al. Observation of Parity-Time Symmetry in Optically Induced Atomic Lattices, *Phys. Rev. Lett.* **117**, 123601 (2016).

[16] Zhang, Y. et al. Optical Bloch Oscillation and Zener Tunneling in an Atomic System, *Optica.* **4**, 571 (2017).

[17] Zhang, Z. et al. Observation of edge solitons in photonic graphene, *Nat. Commun.* **11**, 1902 (2020).

[18] Hang, C. et al. Storage and retrieval of Airy light wave packets in a coherent atomic system, *Phys. Rev. A.* **90**, 023822 (2014).

[19] Zhuang, F. et al. Propagation and modulation of Airy beams through a four-level electromagnetic induced transparency atomic vapor, *Opt. Lett.* **37**, 1871 (2012).

[20] Zhang, Y. et al. Interactions of Airy beams, nonlinear accelerating beams, and induced solitons in Kerr and saturable nonlinear media, *Opt. Express.* **22**, 7160-7171 (2014).

[21] Zhang, Y. et al. Periodic inversion and phase transition of finite energy Airy beams in a medium with parabolic potential, *Opt. Express.* **23**, 10467-10480 (2015).

[22] Shen, M. et al. Solitons shedding from Airy beams and bound states of breathing

Airy solitons in nonlocal nonlinear media, *Sci. Rep*. **5**, 9814 (2015).

[23] Wu, Z. et al. Self-accelerating Airy-Laguerre-Gaussian light bullets in a two-dimensional strongly nonlocal nonlinear medium, *Opt. Express.* **25** 30468-30478 (2017).

[24] Wu, Z. et al. Evolution of finite energy Airy beams in cubic-quintic atomic vapor system, *Front Phys*. **13**, 134201 (2018).

[25] Deng, D. & Deng, F. Three-dimensional localized Airy-Hermite-Gaussian and Airy-Helical-Hermite-Gaussian wave packets in free space, *Opt. Express.* **24**, 5478-5486 (2016).

[26] Zhong, H. et al. Nonparaxial self-accelerating beams in an atomic vapor with electromagnetically induced transparency, *Opt. Lett.* **41**, 5644 (2016).

[27] Schley, R. et al. Loss-proof self-accelerating beams and their use in non-paraxial manipulation of particles' trajectories, *Nat. Commun.* **5**, 5189 (2014).

[28] Kaminer, I. et al. Nondiffracting Accelerating Wave Packets of Maxwell's Equations, *Phys. Rev. Lett.* **108**, 163901 (2012).

[29] Lumer, Y. et al. Incoherent self-accelerating beams, *Optica.* **2**, 886 (2015).

[30] Zhang, Y. & Xiao, M. Multi-Wave Mixing Processes:From Ultrafast Polarization Beats to Electromagnetically Induced Transparency, (HEP & Springer, 2009).

[31] Zhang, L. et al. Propagation dynamics of super-Gaussian beams in fractional Schrödinger equation: from linear to nonlinear regimes, Opt Express **24**, 14406-14418 (2016).

[32] Zhang, Y. et al. Evolution of the Bessel–Gaussian beam modeled by the fractional Schrödinger equation, *J. Opt. Soc. Am. B.* **37**, 3414 (2020).

[33] Wu, Z. et al. Dynamics of Hermite–Gaussian beams in the linear and nonlocal nonlinear fractional Schrödinger equations, *Results Phys.* **16**, 103008 (2020).

[34] Zhang, Y. et al. Diffraction-free beams in fractional Schrödinger equation, *Sci. Rep.* **6**, 23645 (2016).

[35] Kaminer, I. et al. Self-accelerating self-trapped optical beams, *Phys. Rev. Lett.* **106**, 213903 (2011).

[36] Vallée, O. & Soares, M. Airy functions and applications to physics (Imperial College Press, Singapore, 2010), 2nd ed.

[37] Zhang, Y. et al. Soliton pair generation in the interactions of Airy and nonlinear

accelerating beams, *Opt. Lett.* **38**, 4585 (2013).

Acknowledgements

We acknowledge the kind support of National Natural Science Foundation of China (NNSFC) (61805068, 61875053, 62074127), China Postdoctoral Science Foundation (CPSF) (2017M620300), and Science and Technology Department of Henan Province (202102210111).

Author contributions

Z.W. conceived the idea of this paper and guided the research. Z.W., K.Y., F. W. and Y.G. contributed to resources, writing, review and editing of the paper. Z.W., Y. Z. and J. R. performed the numerical simulations and produced all figures.

Competing interests

The authors declare no conflict of interest.

Figures

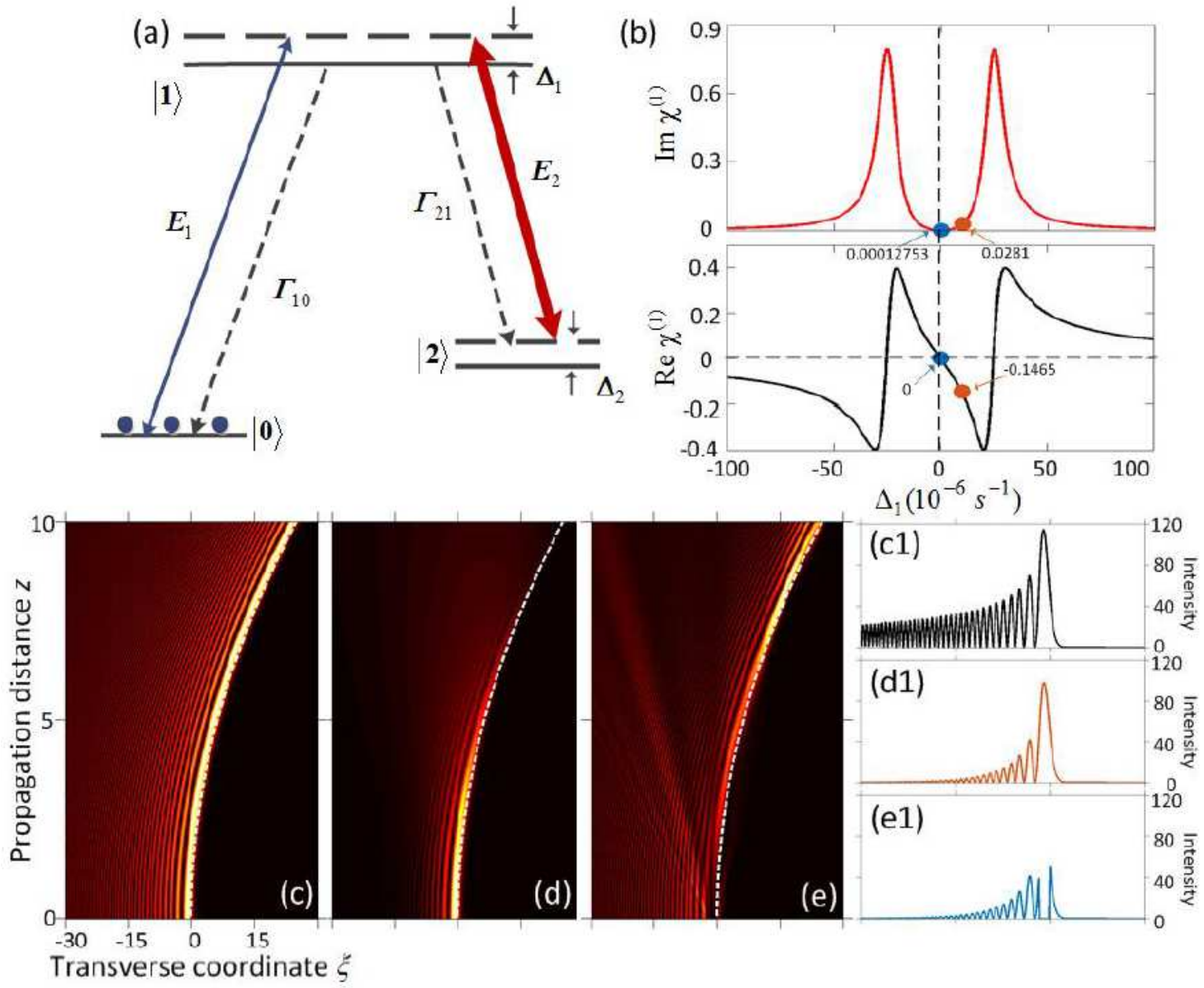

Figure 1

see .pdf for figure caption

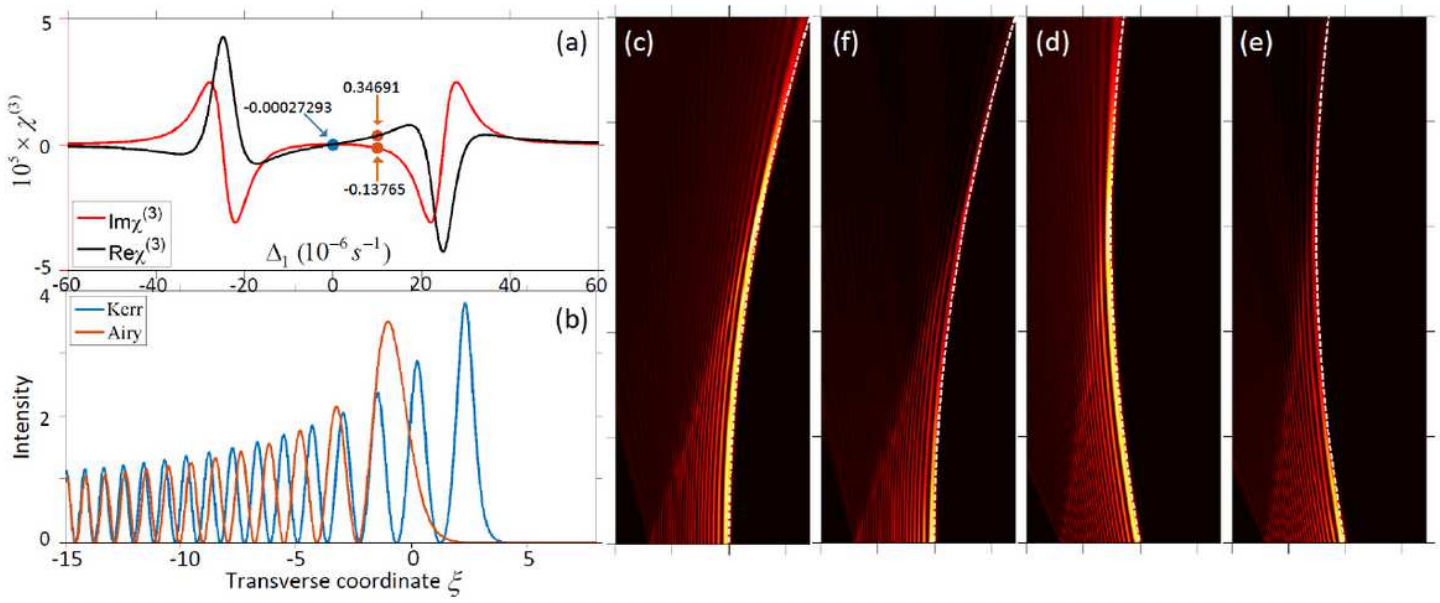

Figure 2

see .pdf for figure caption

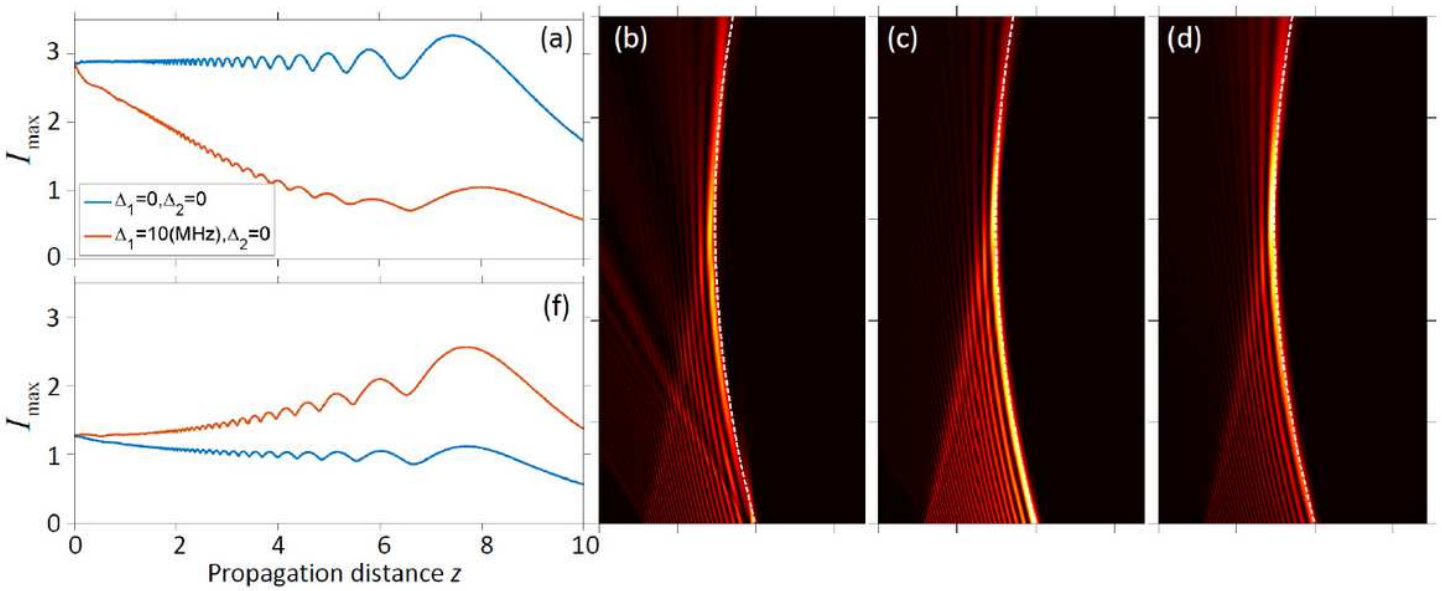

Figure 3

see .pdf for figure caption

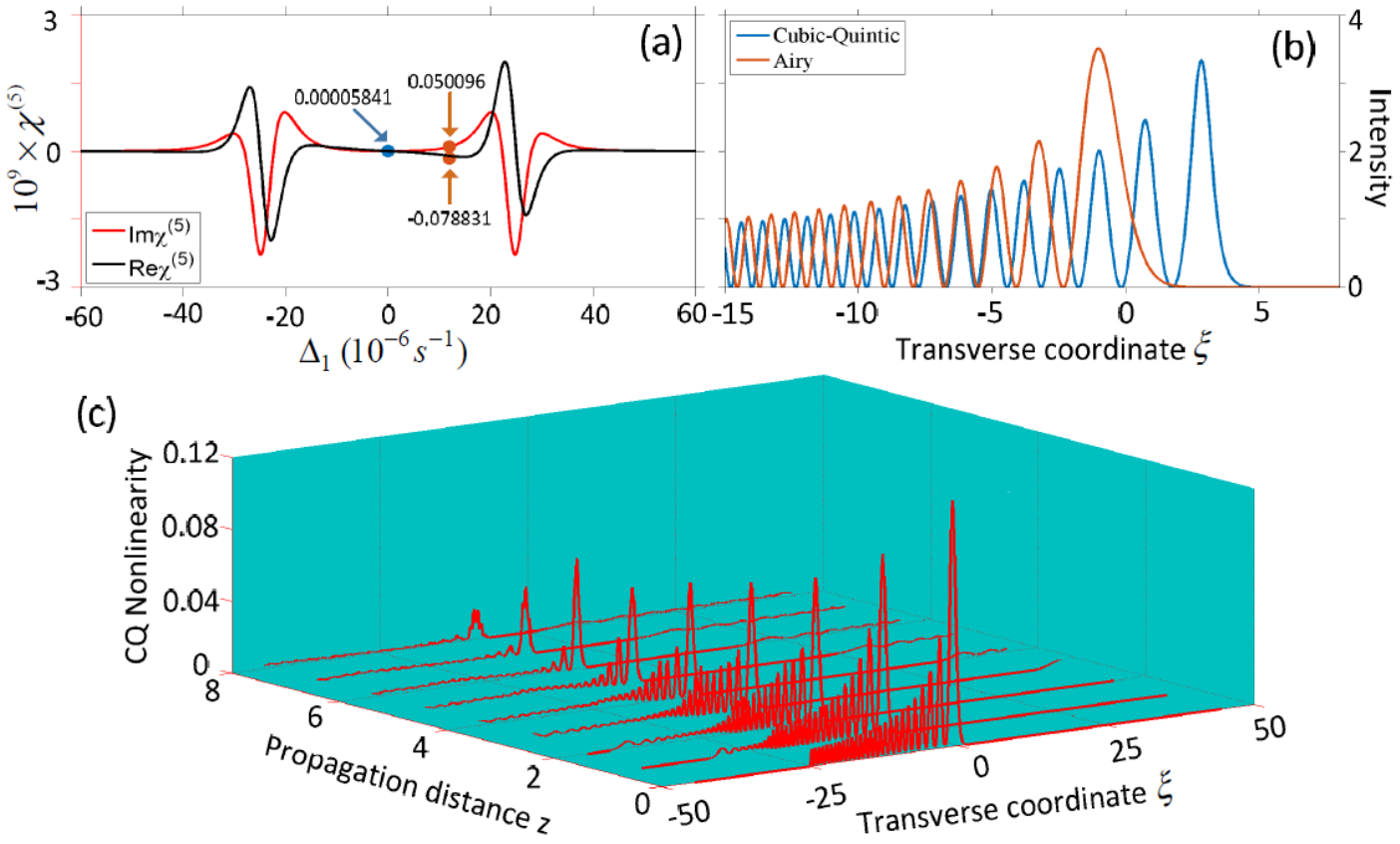

Figure 4

see .pdf for figure caption

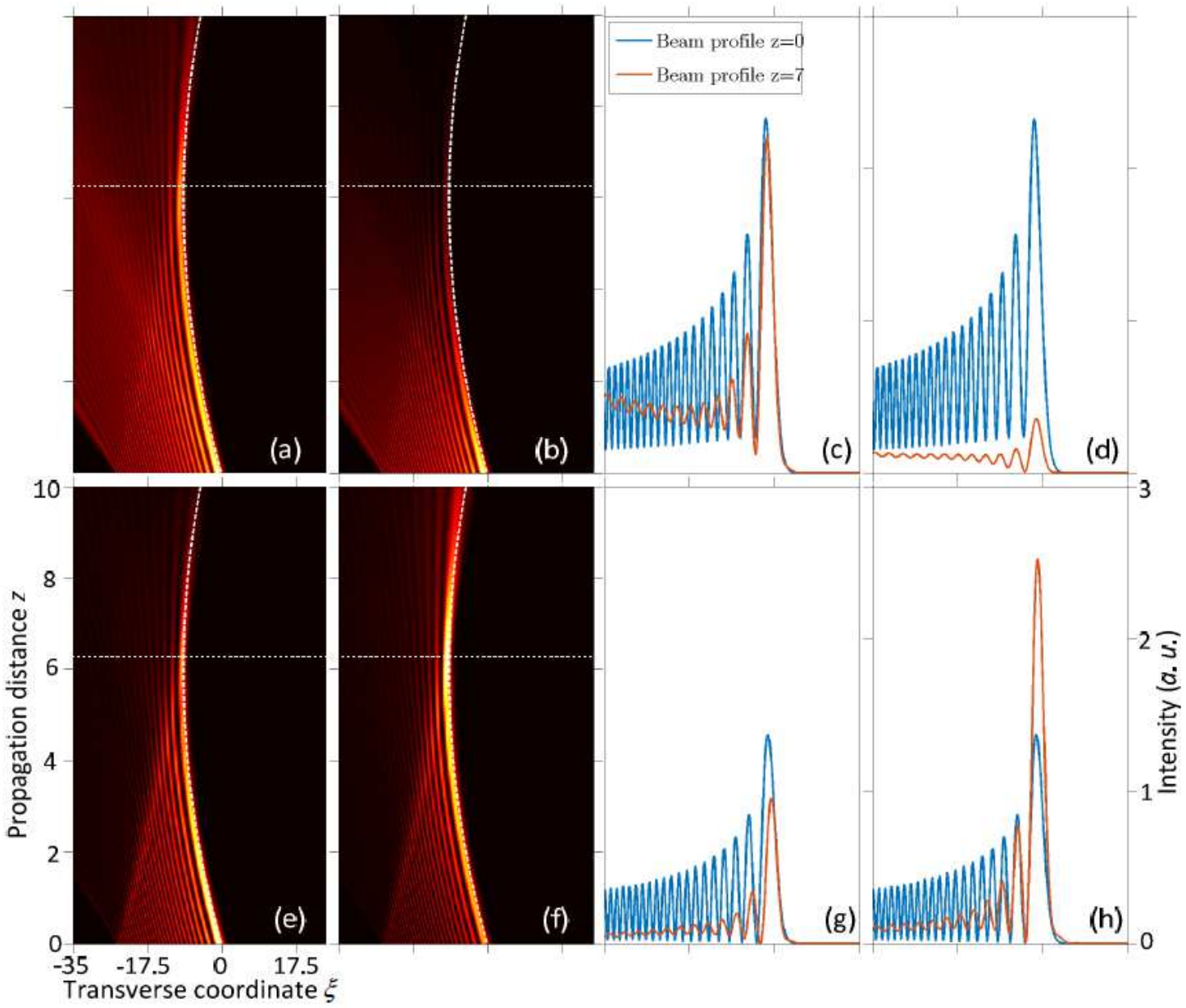

Figure 5

see .pdf for figure caption

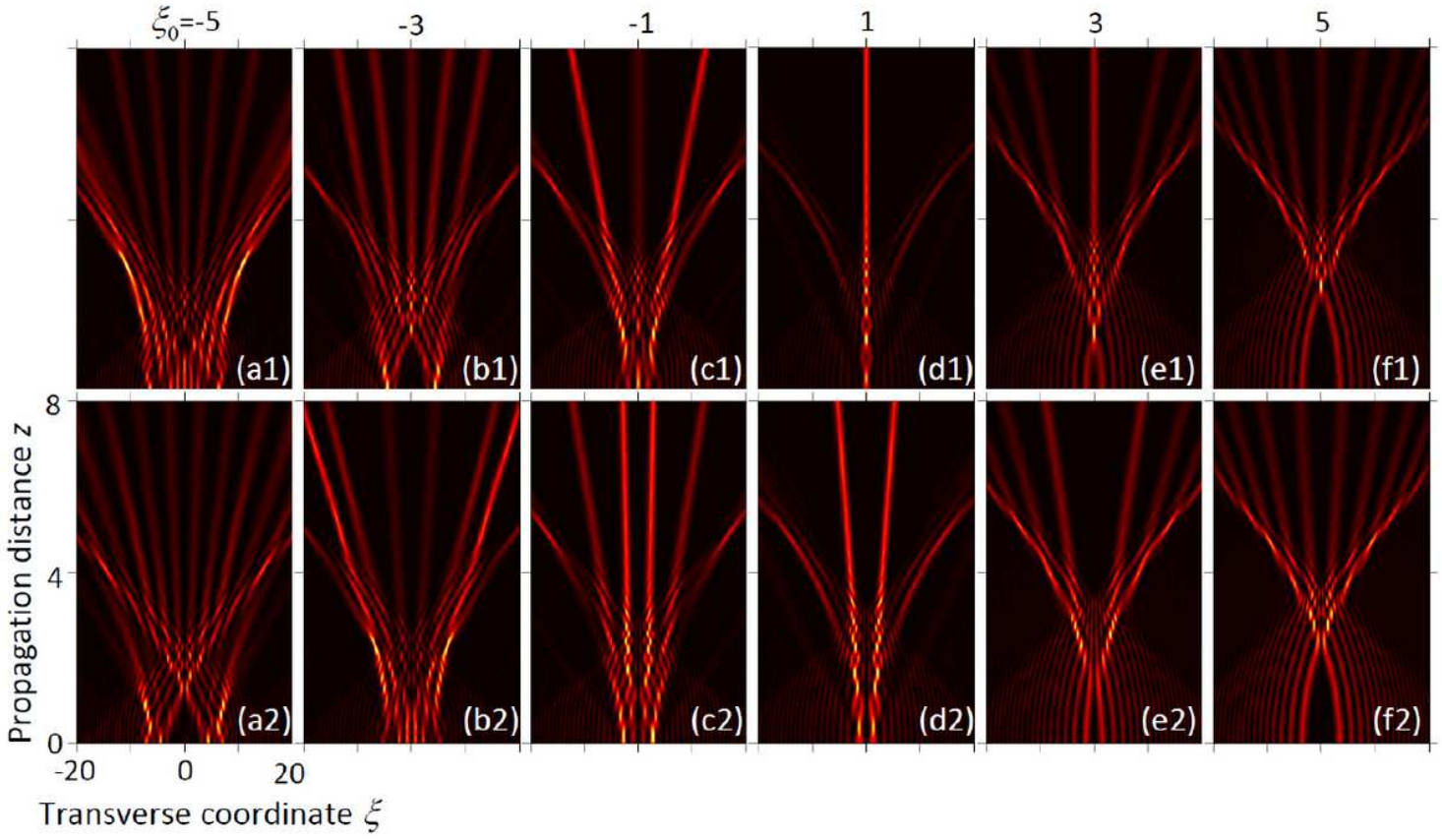

Figure 6

see .pdf for figure caption

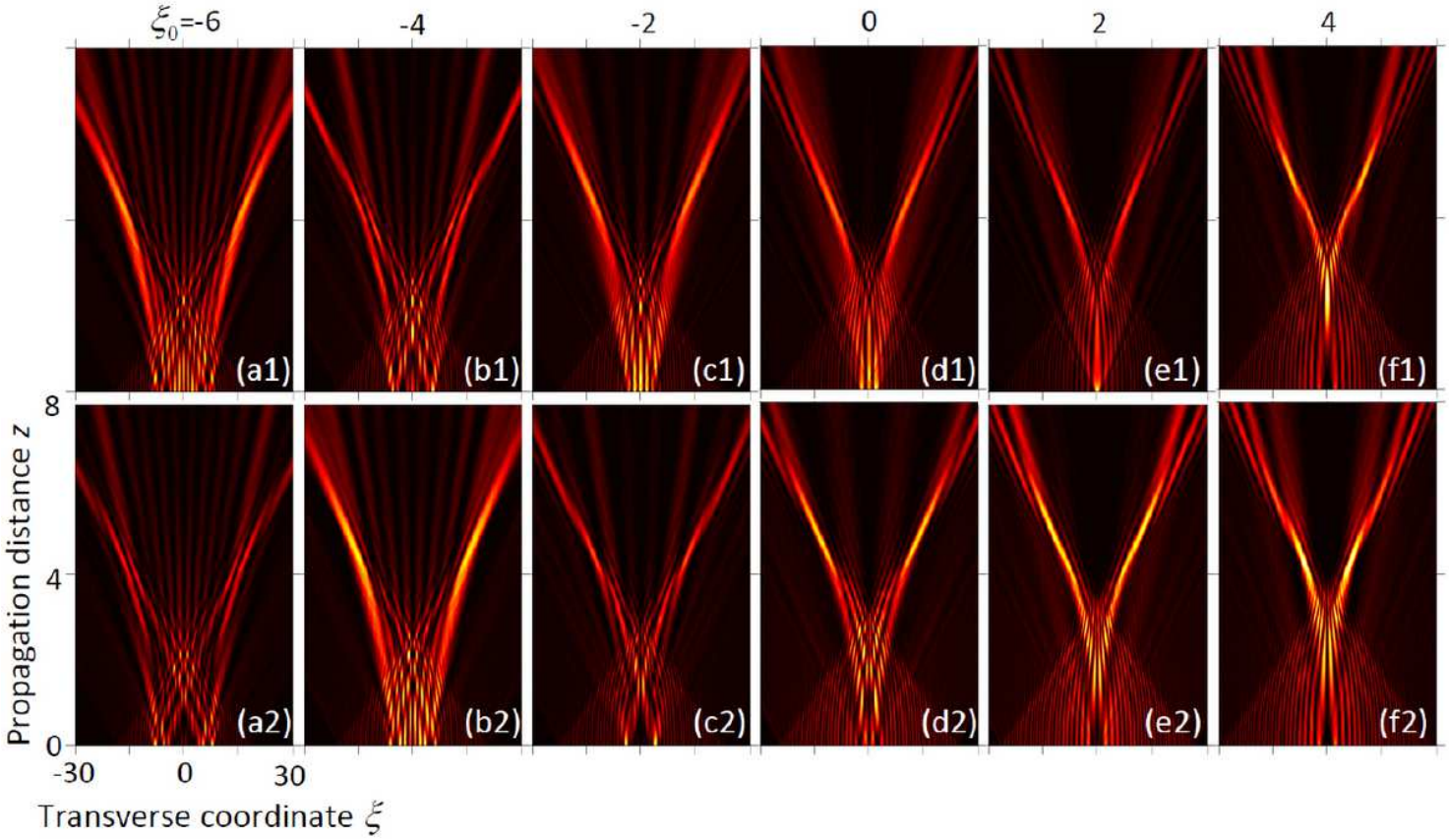

Figure 7

see .pdf for figure caption